Eur Biophys J (2010) 39:1129–1142
DOI 10.1007/s00249-009-0564-4

ORIGINAL PAPER

# Spectral characterization of the recombinant mouse tumor suppressor 101F6 protein

**Alajos Bérczi · Filip Desmet · Sabine Van Doorslaer · Han Asard**

Received: 2 July 2009 / Revised: 29 October 2009 / Accepted: 5 November 2009 / Published online: 27 November 2009


**Abstract** Tumor suppressor protein 101F6, a gene product of the 3p21.3 (human) and 9F1 (mouse) chromosomal region, has recently been identified as a member of the cytochrome *b*561 (Cyt-*b*561) protein family by sequence homology. The $His_6$-tagged recombinant mouse tumor suppressor Cyt-*b*561 protein (TSCytb) was recently expressed in yeast and purified, and the ascorbate reducibility was determined. TSCytb is auto-oxidizable and has two distinct heme *b* centers with redox potentials of ~40 and ~140 mV. Its split α-band in the dithionite-reduced spectrum at both 295 and 77 K is well resolved, and the separation between the two α-peaks is ~7 nm (~222 $cm^{-1}$). Singular value decomposition analysis of the split α-band in the ascorbate-reduced spectra revealed the presence of two major spectral components, each of them with split α-band but with different peak separations (6 and 8 nm). Similar minor differences in peak separation were obtained when the split α-bands in ascorbate-reduced difference spectra at low (<1 mM) and high (>10 mM) ascorbate concentrations were analysed. According to low-temperature electron paramagnetic resonance (EPR) spectroscopy, the two heme *b* centers are in the low-spin ferric state with maximum principal *g* values of 3.61 and 2.96, respectively. These values differ from the ones observed for other members of the Cyt-*b*561 family. According to resonance Raman spectroscopy, the porphyrin rings are in a relaxed state. The spectroscopic results are only partially in agreement with those obtained earlier for the native chromaffin granule Cyt-*b*561.

**Keywords** Ascorbate · Auto-oxidation · Cyt-*b*561 protein · EPR · Raman · UV–VIS · 101F6 protein

A. Bérczi (✉)
Institute of Biophysics, Biological Research Center, Hungarian Academy of Sciences, Temesvári krt. 62, P.O. Box 521, 6701 Szeged, Hungary
e-mail: berczi@brc.hu

F. Desmet · S. Van Doorslaer
Department of Physics, University of Antwerp, Campus Drie Eiken, Universiteitsplein 1, 2610 Wilrijk, Belgium

H. Asard
Department of Biology, University of Antwerp, Campus Groenenborger, Groenenborgerlaan 171, 2020 Antwerpen, Belgium

## Introduction

Cytochromes *b*561 (Cyts-*b*561) constitute a newly identified family of integral membrane proteins. These are *trans*-membrane ascorbate (ASC)-reducible two-heme proteins with six *trans*-membrane helices (Tsubaki et al. 2005). There are four well-conserved His residues located in four consecutive *trans*-membrane α-helices for binding of the two hemes. Such proteins have recently been identified in a great variety of organisms, including invertebrates, vertebrates, and plants (Asard et al. 2001; Bashtovyy et al. 2003; Verelst and Asard 2003; Tsubaki et al. 2005). The first member of the Cyt-*b*561 protein family that was discovered is the chromaffin granule cytochrome *b*561 (CGCytb). This protein was found to function as an electron transporter providing electrons from cytosolic ASC to intravesicular dopamine β-hydroxylase (Flatmark and Terland 1971; Kelley and Njus 1986; Kent and Fleming 1987; Fleming and Kent 1991). CGCytb was first purified from bovine adrenal glands (Apps et al. 1980; Flatmark and Grønberg 1981; Wakefield et al. 1984) and its physico-chemical properties were established (Apps et al. 1984; Tsubaki et al. 1997; Takeuchi et al. 2001, 2004). The bovine and mouse

CGCytb have recently been cloned and expressed in yeast, insect, and bacterial cells (Bérczi et al. 2005; Liu et al. 2005, 2007), and the recombinant proteins have been purified and characterized; their physico-chemical properties are identical to the native bovine protein.

Three mammalian and one plant Cyts-*b*561, namely CGCytb, the duodenal Cyt-*b*561 (DCytb; [McKie et al. 2001]), the lysosomal Cyt-*b*561 (LCytb; Zhang et al. 2006), and the tonoplast Cyt-*b*561 (TCytb; Griesen et al. 2004) showed ASC-dependent *trans*-membrane ferrireductase activity when expressed in yeast cells (Su and Asard 2006; Bérczi et al. 2007). However, only DCytb has been demonstrated to be involved in animal iron metabolism (McKie et al. 2001). CGCytb participates in ASC regeneration, while the biological function of LCytb and TCytb has not yet been elucidated.

A human tumor suppressor protein (the 101F6 protein) has also been identified as putative member of the Cyts-*b*561 (Lerman and Minna 2000; Ponting 2001; Tsubaki et al. 2005). The mouse orthologue was also identified and shown to be 85 and 95% identical to the human sequences at the cDNA and protein sequence level, respectively (Lerman and Minna 2000). Both proteins have six *trans*-membrane α-helices with (1) 222 residues, (2) the N- and C-termini in the cytoplasm, and (3) four well-conserved histidine residues for (4) binding with two heme *b* prosthetic groups. The 101F6 mRNA was widely expressed in tissues, and the mouse mRNA was especially abundant in liver, kidney, and lung (Mizutani et al. 2007), while the human protein was most abundant in liver, placenta, and lung (Lerman and Minna 2000). Elevated expression of *101F6* in tumor cells significantly inhibited cell growth; and intratumoral injection of recombinant adenovirus-*101F6* gene vectors as well as systemic administration of protamine-complexed adenovirus-*101F6* gene vectors significantly suppressed tumor xenograft growth (Ji et al. 2002). Ohtani et al. (2007) recently found that nanoparticle-mediated *101F6* gene transfer and a subpharmacological concentration of ASC synergistically and selectively inhibited tumor cell growth by caspase-independent apoptosis and autophagy both in vitro and in vivo. c-Myc-tagged mouse 101F6 protein has recently been expressed in Chinese hamster ovary cells, and immunofluorescence microscopy was used to localize the recombinant proteins; they were found in small vesicles, including endosomes and endoplasmic reticulum of the perinuclear region (Mizutani et al. 2007). The $His_6$-tagged mouse orthologue, called TSCytb, and the $His_8$-tagged human 101F6 protein have very recently and independently been expressed in yeasts, and the highly purified proteins showed typical Cyt-*b*561 spectra both in their oxidized and ASC- or dithionite-reduced forms (Bérczi and Asard 2008; Recuenco et al. 2009).

To better understand the molecular action mechanism of TSCytb and its role in tumor suppression, we studied in detail the spectral properties of the two heme groups embedded in the protein and essential for its function. In this paper we provide evidence for the mouse TSCytb to be a two-heme-containing *b*-type cytochrome and identify the differences between TSCytb and other previously characterized Cyt-*b*561 proteins.

## Materials and methods

### Cell growth, membrane preparation, protein purification

Yeast cell growth, microsomal membrane preparation, and protein purification by affinity chromatography were performed as detailed previously (Bérczi and Asard 2008). Briefly, mouse TSCytb (the sequence corresponds to GenBank protein entry NP_062694) with a C-terminal $His_6$-tag was cloned into a pESC-His expression vector (Stratagene, La Jolla, CA, USA) and grown in yeast cells (*Saccharomyces cerevisiae*, strain YPH499: ura3-52 lys2-801$^{amber}$ade2-101$^{ochre}$ trp1-Δ63 his3-Δ200 leu2-Δ1) according to the manufacturer's instructions (Stratagene) at 30°C in a benchtop incubator shaker (Excella E24R, New Brunswick Scientific, Edison, NJ, USA). Cells were broken by a bead-beater (Biospec Products, Bartlesville, OK, USA), and the stripped microsomal membrane fraction was obtained by differential centrifugation steps. Membrane vesicles were solubilized by sucrose monolaurate (SML; Dojindo, Tokyo, Japan) and the $His_6$-tagged recombinant mouse TSCytb (hereafter TSCytb) was purified to almost homogeneity by affinity chromatography using Ni–NTA His-Bind resin (Novagen, Madison, WI, USA). Purified TSCytb was stored in phosphate buffer [50 mM $NaH_2PO_4$, pH 7, 10% (w/v) glycerol, 0.1% (w/v) SML] at −80°C until use. The very same phosphate buffer was used in all spectroscopy.

Protein was measured according to Markwell et al. (1978), using BSA as the standard and deoxycholate as detergent in the presence of phosphate buffer and SML both in standards and in samples.

### UV–VIS spectroscopy and redox titration

Absorption spectra, time-dependent absorbance changes at fixed wavelength, and optical redox titration were recorded at room temperature in split beam mode (with appropriate buffer as reference) with an OLIS-updated SLM-Aminco DW2000 spectrophotometer (OLIS, Bogart, GA, USA) with 2 nm slit width and under continuous stirring. The cuvette was equipped with a homemade lid for housing the

reference electrode (customized EE009 "no leak" Ag/AgCl reference mini-electrode, Sypress Systems, Chelmsford, MA, USA), the platinum electrode, the gas inlet and outlet, and an inlet for additions. Anaerobic conditions were created by continuous streaming of humidified $N_2$ or Ar gas over the solution in the cuvette. Anaerobic measurements started after 15–20 min of equilibration of the solution in the cuvette. The spectrum of oxidized TSCytb was always recorded first and the dithionite-reduced spectrum was recorded last. When improvement of the signal-to-noise ratio was needed, multiple scans were averaged. If mentioned, the cytochrome *b* content was always calculated from the dithionite-reduced minus ferricyanide-oxidized difference spectra by using a millimolar extinction coefficient of $\varepsilon_{561\text{nm}} = 30\ \text{mM}^{-1}\ \text{cm}^{-1}$ (Tsubaki et al. 1997; Liu et al. 2005).

Optical redox titration was performed in phosphate buffer (see above) under Ar atmosphere at room temperature as detailed elsewhere (Bérczi et al. 2005). Redox mediators used at 20 μM concentration each were potassium ferricyanide (+430 mV), 3,6-diaminodurol (+275 mV), FeNaEDTA (+140 mV), phenazine methosulfate (+85 mV), duroquinone (+5 mV), 2-hydroxy-1,4-naphthoquinone (−145 mV), and ridoflavin-5′-monophosphate (−219 mV). Reductive titration was performed by stepwise addition of sodium dithionite (5 mM) by a Hamilton syringe. The α-band was recorded between 540 and 580 nm at appropriate intervals, and reduced-minus-oxidized difference spectra were used in data analyses. For obtaining the redox titration curve, each difference spectrum was integrated between 548 and 570 nm, the maximum of these values was taken to represent 100%, and other values were expressed in relation to this reference value. Experimental points were then approximated by Nernst equation assuming the presence of two one-electron redox centers.

Spectrum analysis was performed by using Origin8E software and/or SPSERV V3.5 (copyright Csaba Bagyinka; see Branca et al. 2007).

### Resonance Raman spectroscopy

Resonance Raman (RR) measurements were carried out on a Dilor XY-800 Raman scattering spectrometer (Lille, France) consisting of a triple 800 mm spectrograph, operating in low-dispersion mode with CCD detection. Spectra were recorded at room temperature. The excitation source was a mixed gas Kr/Ar ion laser (Spectra-Physics BeamLok 2060, Mountain View, CA, USA) operating at 413.1 nm. The protein solution was stirred at 500 rpm to avoid local heating and photochemical decomposition in the laser beam. Ten spectra (90–120 s recording time each) were acquired to allow the removal of cosmic ray spikes. This was done by eliminating the lowest and highest data points for each frequency value and averaging the remaining values. Laser powers in the range of 0.5–60 mW were used. Samples with protein concentrations between 0.4 and 0.7 mg $\text{ml}^{-1}$ (pH 7.0, at 20°C) were employed.

The dithionite-reduced form of TSCytb was obtained by flushing the volume above the protein solution (1 ml) by nitrogen in a cuvette that was sealed air-tight with a septum. Afterwards 10 μl of 200 mM sodium dithionite in phosphate buffer was added to the cuvette with a Hamilton syringe.

### EPR spectroscopy

The X-band (microwave frequency of 9.43 GHz) continuous-wave (CW) electron paramagnetic resonance (EPR) spectra of TSCytb in detergent micelles and in phosphate buffer were recorded on a Bruker ESP300E spectrometer (Rheinstetten, Germany) equipped with a gas-flow cryogenic system (Oxford Inc., Oxford, UK), allowing for operation from room temperature down to 2.5 K. The magnetic field was measured with a Bruker ER035 M NMR Gaussmeter (Rheinstetten, Germany). The presented CW-EPR spectra were recorded with a microwave power of 2 mW, modulation amplitude of 0.5 mT, and modulation frequency of 100 kHz. The EPR tubes with the frozen sample solution were attached to a vacuum line during the EPR experiment in order to remove the paramagnetic $O_2$. The EPR spectra were simulated using EasySpin (Stoll and Schweiger 2006), a toolbox for the MATLAB program.

## Results

### UV–VIS spectroscopy

TSCytb has recently been expressed in yeast (*Saccharomyces serevisiae*) cells and purified to almost homogeneity in detergent (sucrose monolaurate-containing) micelles (Bérczi and Asard 2008). It was also shown that a $\text{His}_6$ tag on the C-terminus did not influence the UV–VIS spectra of the protein in the 500–600 nm region. Although the presence of a split α-band in the spectra of reduced TSCytb was evident already at room temperature, the two α-peaks become clearly separated in the low-temperature spectra measured at 77 K (Fig. 1a). When reduced-minus-oxidized difference spectra obtained at room (297 K) and low (77 K) temperatures were compared (Fig. 1b), the characteristic wavelength shifts of the absorption peaks in the split α-band were well resolved. As revealed by spectrum analysis, the separation between the two peaks of the split α-band is ∼7 nm (∼222 $\text{cm}^{-1}$), both at 297 and 77 K, and the two maxima shift 2.5 nm towards lower wavelengths (blue-shift) with decreasing temperature.

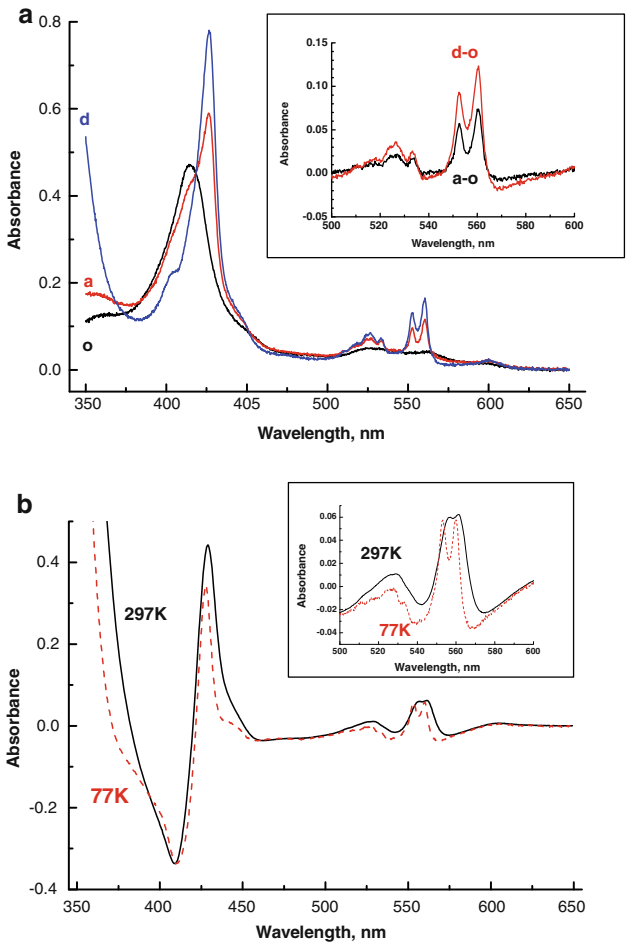


**Fig. 1a, b** UV–VIS spectra of TSCytb in SML micelles in phosphate buffer at pH 7. **a** Spectra of fully oxidized (*o*), ascorbate reduced (50 mM, *a*), and dithionite reduced (5 mM, *d*) TSCytb were recorded with 2 nm slit width, 50 nm/min scan rate, 2 mm optical path at 0.5 mg/ml protein concentration, and 77 K. The *inset* shows the split α-band in the (α + β)-band region (500–600 nm) of the reduced-minus-oxidized difference spectra. **b** Comparison of the dithionite reduced-minus-oxidized difference spectra of TSCytb recorded at 77 and 297 K. The optical path was 2 and 10 mm for the 77 and 297 K measurements, respectively. Otherwise all parameters were identical to **a**

## Ascorbate-dependent reduction

We showed earlier that the reduction of TSCytb by ascorbate did not saturate even at 75 mM ascorbate (Bérczi and Asard 2008). The split α-band in the absolute spectra of ascorbate-reduced TSCytb obtained at room temperature (Fig. 2a) was analyzed at low ascorbate ([ASC] < 1 mM) and high ascorbate ([ASC] > 10 mM) concentrations using the method of Kamensky et al. (2007). A high-affinity (HA) spectrum and a low-affinity (LA) spectrum were resolved (Fig. 2b).

Spectrum analysis revealed that both spectra have a split α-band with 8 and 6 nm peak separations, respectively (Fig. 3a, b). Furthermore, when the whole set of absolute spectra of ascorbate-reduced TSCytb was subjected to a singular value decomposition (SVD) analysis (Shrager 1986; Henry and Hofrichter 1992), two main SVD components (SVD1 and SVD2) were resolved (Fig. 2c, d). Spectrum analysis of these two SVD component spectra revealed again the presence of two peaks in each SVD component spectrum with very similar peak separations to those of the HA and LA component spectra (Fig. 3c, d).

Table 1 contains the summary of spectral parameters obtained for the component spectra in the two different spectrum analyses. Note that the accuracy given in Table 1 serves as a measure of the reproducibility and consistency of the different decomposition analyses but does not take into account the general experimental error introduced in all measurements by the use of a 2 nm slit width.

## Auto-oxidation

There are two indications that TSCytb is an auto-oxidizable cytochrome. First, if no ascorbate is present in the buffer, or if the ascorbate-containing buffer is exchanged with an ascorbate-free buffer by a fast desalting chromatography step at the end of the purification procedure, the highly purified protein is always in its oxidized form. Secondly, when the absorption of freshly prepared dithionite-reduced TSCytb is monitored in air at the Soret band, the absorbance at 428 nm changes only slightly for a while, and then suddenly and sharply drops, followed by a slower phase of gradual decrease (Fig. 4a). When the redox potential of the medium is monitored in parallel with the absorbance change, the very low redox potential at the start of the experiment (in the presence of dithionite in the cuvette) gradually increases at an increasing rate. At the time point where the fast absorbance change at 428 nm starts, the rate of the redox-potential change reaches a maximum. The redox-potential value levels off at a high redox-potential value, as the absorbance change becomes small (Fig. 4a). Above a certain initial dithionite concentration (~0.6–0.7 mM), the phenomenon described above is independent of the initial amount (concentration) of dithionite added; only the duration of the very first slow absorbance change increases with increasing initial concentration of dithionite applied. If the absorbance is plotted as a function of the redox potential, a typical redox titration curve is obtained (Fig. 4b). The experimental points fit very well to the theoretical curve obtained using a Nernstian equation and assuming that there are two one-electron redox centers in TSCytb with different redox potentials (+22 and +147 mV). This phenomenon does not occur when humidified nitrogen or argon gas is continuously present in the cuvette.

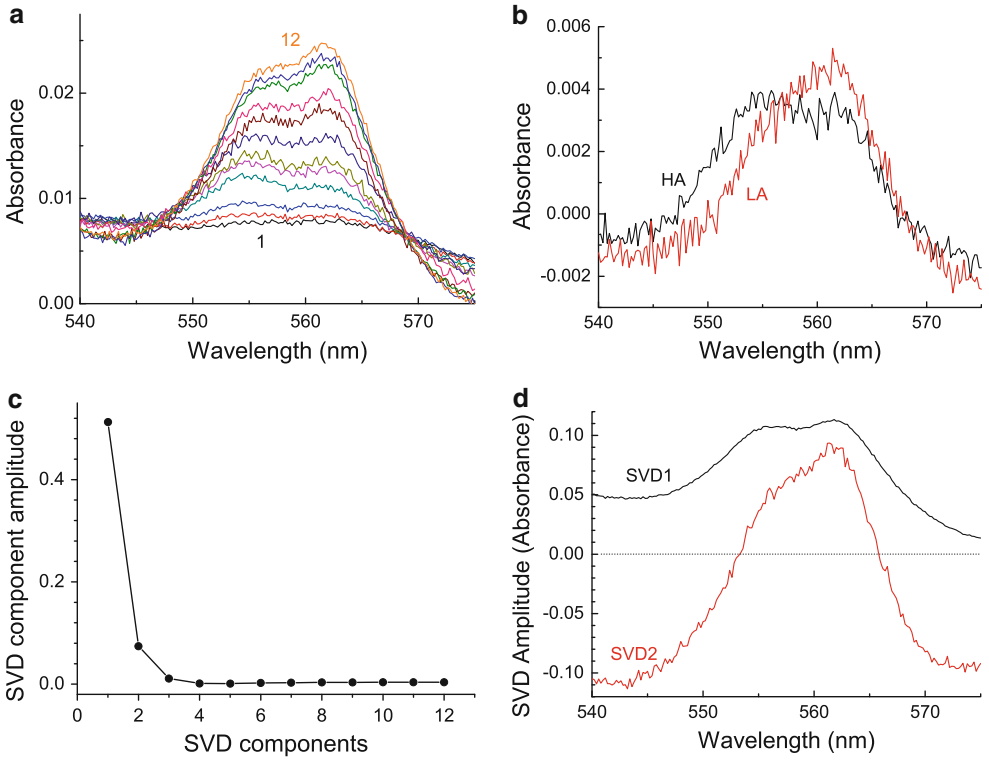


**Fig. 2a–d** Ascorbate-dependent reduction of TSCytb in SML micelles in phosphate buffer at pH 7 and 297 K. Steady-state spectra were recorded in the presence of 0, 0.004, 0.044, 0.444, 0.844, 1.64, 3.64, 7.64, 15.6, 35.6, 75.6, and 115 mM ascorbate [from *bottom* (trace 1) to *top* (trace 12), respectively]. Only the split α-band region is shown (**a**). The high-affinity (HA) and the low-affinity (LA) component spectra were obtained by subtracting trace 3 from trace 5 and trace 8 from trace 12, respectively (**b**). The SVD analysis of spectra shown in **a** resulted in two major components (**c**; the diagonal matrix elements, $s_{jj}$, or the singular values are presented). Spectra of these major SVD components (SVD1 and SVD2) are shown in **d**

## Optical redox titration

The presence of two hemes with different redox potentials is characteristic for Cyt-*b*561 proteins. Although analysis of the results of the auto-oxidation experiment has provided two distinct redox potential values, these values need verification by conventional redox titrations. Using a broad range of redox mediators and dithionite, the presence of two one-electron redox centers in TSCytb was verified by optical redox titration under anaerobic conditions (Fig. 5). Analysis of the experimental values resulted in +43 and +141 mV (with ±9 mV uncertainty in these fitting parameters) for the redox potentials of the two hemes in TSCytb. These are reasonably close to those obtained from the auto-oxidation experiments or to those published for other Cyts-*b*561 proteins (about +50 and +150 mV; Apps et al. 1984; Takeuchi et al. 2001, 2004; Bérczi et al. 2005, 2007). However, they are considerably higher than those obtained for the human recombinant tumor suppressor 101F6 protein (about +10 and +100 mV; Recuenco et al. 2009).

## Resonance Raman spectroscopy

The RR spectra of TSCytb in oxidized (as expressed or ferric) and dithionite-reduced (or ferrous) states are shown in Fig. 6a, b. The high-frequency region of the RR spectra of the heme proteins contains a number of well-known marker bands that are sensitive to the oxidation state, the spin state, and the coordination of the heme iron (Lou et al. 2000). The $\nu_4$, $\nu_3$, and $\nu_2$ bands of ferrous TSCytb are located at 1,357, 1,492, and 1,580 $cm^{-1}$ (Fig. 6b). These indicate the presence of low-spin ($S = 0$) hexa-coordinated Fe(II) heme in the sample. The band at 1,466 $cm^{-1}$ is due to the buffer. The oxidized form of TSCytb displays clear $\nu_4$, $\nu_3$, and $\nu_2$ bands located at 1,373, 1,501, and 1,578 $cm^{-1}$, typical of low-spin hexa-coordinated ferric heme (Fig. 6b). In addition, the RR spectrum of the as-expressed TSCytb shows the same marker bands as the reduced form of the protein, which is most notably seen for the $\nu_4$ band (Fig. 6b). The intensity of the $\nu_4$ band at ~1,361 $cm^{-1}$ increases with increasing laser power, pointing to the occurrence of photoreduction,

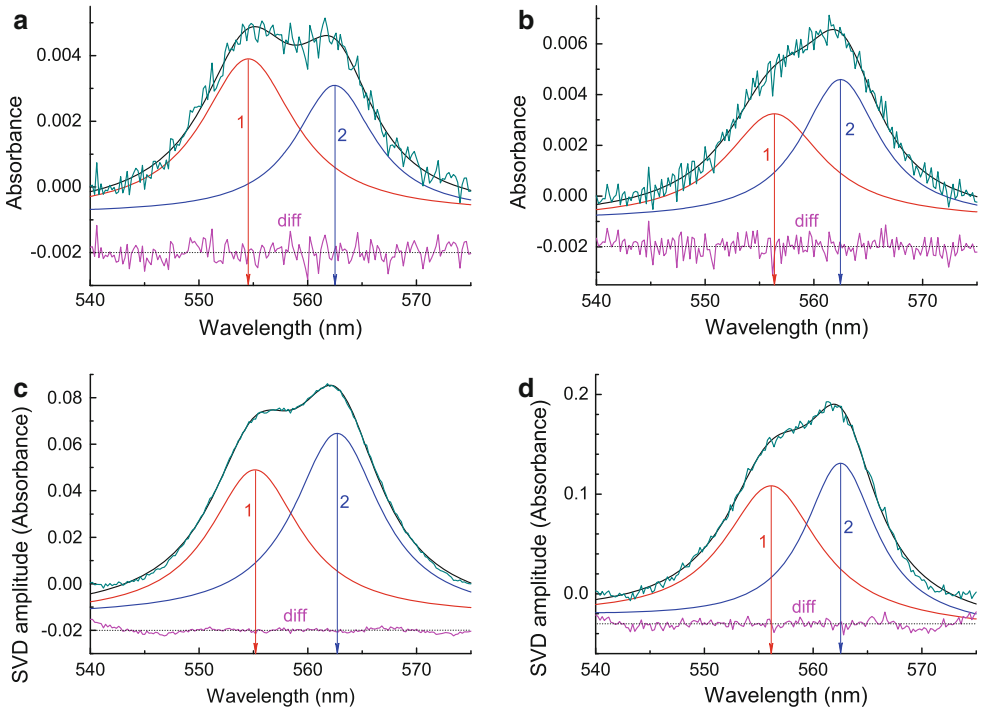


**Fig. 3** Fitting with double Lorentzian curves of HA and LA spectra (**a** and **b**) as well as of SVD1 and SVD2 component spectra (**c** and **d**). The difference spectrum (*diff*) in each case was obtained by subtracting the fitted curve from the spectrum under analysis (for clarity, its position was down shifted on the graphs and the zero line is represented by a *dotted line*). Fitted Lorentzian curves are labeled as *1* for the component with the lower peak wavelength and *2* for the component with the higher peak wavelength

**Table 1** Spectral parameters obtained by analyzing (simulating with double Lorentzian curves) the absolute spectra of ascorbate-reduced TSCytb at different ascorbate concentrations (see Fig. 2a)

| Name of component spectrum | α-Peak component (nm) | |
|---|---|---|
| | Peak 1 | Peak 2 |
| HA heme spectrum | 554.4 ± 0.1 | 562.4 ± 0.1 |
| LA heme spectrum | 556.2 ± 0.2 | 562.4 ± 0.1 |
| SVD1 spectrum | 554.8 ± 0.2 | 562.6 ± 0.2 |
| SVD2 spectrum | 555.6 ± 0.2 | 562.5 ± 0.1 |
| High-potential heme spectrum[a] | 555.6 | 561.3 |
| Low-potential heme spectrum[a] | 557.7 | 561.6 |

Data (mean ± SD) are from three independent analyses. Peak 1 is always the α-peak component at lower wavelength in the split α-band

[a] Spectral data were calculated from Fig. 4b in Kamensky et al. (2007)

as also reported for other ferric cytochrome and porphyrin systems (Hurst et al. 1991; Terekhov and Kruglik 1995). Note that it proved impossible to fully photo-reduce the system and that the fraction of photoreduction did not change anymore for laser powers higher than 40 mW. At that point, the fraction of ferric to ferrous heme was 2:1 as obtained from a fit of the $\nu_4$ band with a sum of two Lorentzian functions.

The assignment of the Raman bands in the low-frequency part of the spectra is based on the work of Spiro and co-workers on myoglobin (Hu et al. 1996) and cytochrome *c* (Hu et al. 1993), and we use here the notation for the Raman modes adopted by these authors. The depolarized band at 750 $cm^{-1}$ in the spectrum of reduced TSCytb (Fig. 6a) is assigned to the $\nu_{15}$ and $\nu_{16}$, the pyrrole breathing and deformation modes (Hu et al. 1996; Takeuchi et al. 2004). The band at ~383 $cm^{-1}$ is assigned to a propionate bending mode $\delta(C_\beta C_c C_d)$; the frequency of this mode is related to the strength of the hydrogen bonds between the propionate and nearby amino acids. A frequency of 383 $cm^{-1}$ corresponds to strong hydrogen bonding (Uchida et al. 2005). In the oxidized form of TSCytb, two modes are visible around this position, one at 379 $cm^{-1}$ and one at 392 $cm^{-1}$ (Fig. 6a). While the band at 379 $cm^{-1}$ still corresponds to strong hydrogen bonding between the propionate groups and surrounding residues, a frequency of 392 $cm^{-1}$ is too high to be related to a propionate mode (Cerda-Colon et al. 1998). No clear splitting of the vinyl bending modes, $\delta(C_\beta C_a C_b)$, can be observed; we observed a single peak at 414 (418) $cm^{-1}$ of the oxidized (reduced) form of TSCytb. The bending modes of the two vinyl groups of both hemes thus coincide. This can be related to a lack of the out-of-plane distortions of both hemes in TSCytb, i.e., a relaxed heme configuration (Dewilde et al. 2006).

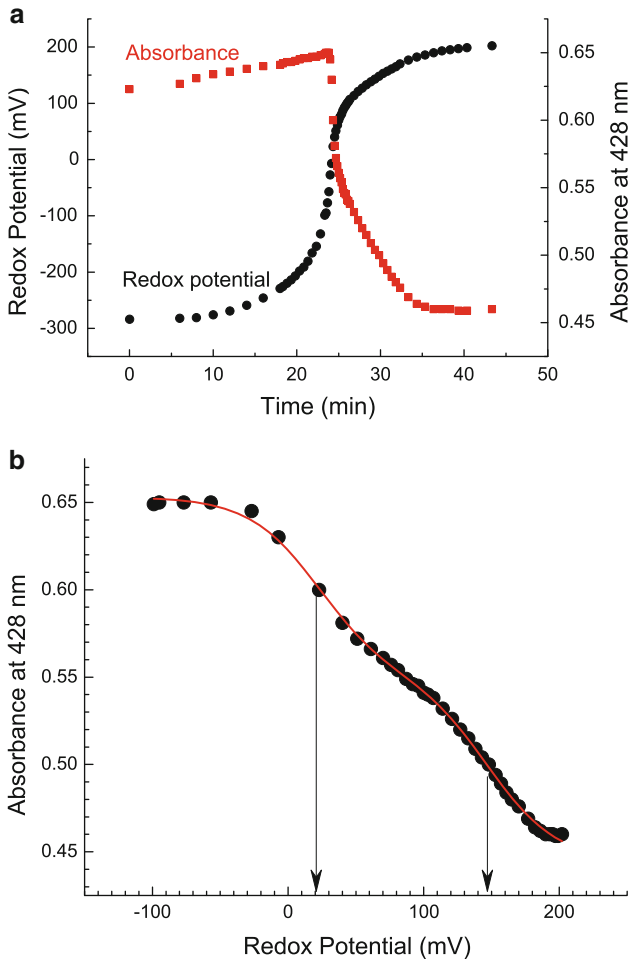


**Fig. 4a, b** Auto-oxidation of TSCytb in SML micelles in phosphate buffer at pH 7 at 297 K. The absorbance change at 428 nm and redox potential were recorded in parallel (**a**) after addition of dithionite to the optical cuvette containing 0.5 mg/ml TSCytb, under continuous stirring in air. When the absorbance change at 428 nm was plotted as a function of redox potential (**b**), a typical redox titration curve was obtained. The experimental points were fit with a Nernstian equation assuming two one-electron redox centers with different redox potentials (continuous curve)

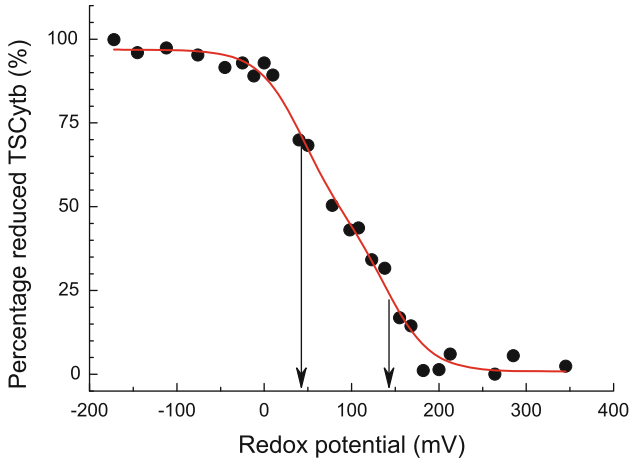


**Fig. 5** Redox titration of TSCytb in phosphate buffer (pH 7) containing 0.1% (w/v) sucrose monolaurate as detergent. Redox titration was performed under anaerobic conditions by recording the α-band spectrum between 540 and 580 nm with increasing dithionite concentration. TSCytb concentration was 1.2 μM. For data analysis, the reduced-minus-oxidized difference spectra were integrated between 548 and 570 nm and the difference between the maximum and minimum values was taken as reference (100%) value; titration is shown as the percentage of reduced TSCytb vs. bulk potential in the assay. The curve was calculated by using +43 and +141 mV redox potential values in the Nernstian equation and assuming the presence of two one-electron redox centers

## EPR spectroscopy

EPR spectra were recorded for the oxidized TSCytb in detergent micelles and 50 mM phosphate buffer (pH 7) at 5, 10, 15, and 30 K (Fig. 7). A simulation of the spectrum reveals the presence of five different components. The signal at $g = 4.28$ indicated with an asterisk in Fig. 7 is typical of extra-heme iron and is of no interest for the further discussion (Takeuchi et al. 2004). Furthermore, an EPR contribution labelled LS1 is observed with principal $g$-values of $g_z = 2.96$, $g_y = 2.26$, and $g_x = 1.46$, where $g_x$ was estimated using the rough approximation that $g_x^2 + g_y^2 + g_z^2 = 16$ (Walker 1999). The EPR parameters of LS1 are typical of a low-spin ferric heme complex. They can be related to the ligand-field parameters $V/\Delta = 0.58$ and $\Delta/\lambda = 3.09$ via Taylor's formulae (Taylor 1977) with $V$ the rhombic splitting parameter, $\Delta$ the tetragonal splitting parameter, and $\lambda$ the spin–orbit coupling. Using Blumberg and Peisach's truth tables (Blumberg and Peisach 1971), these ligand-field parameters can give a rough indication of the identity of the heme iron's axial ligands. The principal $g$-values of LS1 indicate a bis-His coordination of the heme; the ligand-field parameters fall exactly within the 'H-type' region in the truth tables characteristic of hemes with a histidine as fifth ligand and an aromatic or imino nitrogen sixth ligand (Blumberg and Peisach 1971). The EPR signal of LS1 is no longer visible in EPR spectra recorded at temperatures above 50 K (data not shown).

The signal with $g_{max} = 3.61$, labelled LS2, can only be found at temperatures up to 15 K. Only the low-field feature of this rhombic signal is clearly resolved, typical of a so-called highly anisotropic low spin (HALS) ferric heme species (Walker 1999). The fourth major component, labelled HS, in the EPR spectrum of ferric TSCytb stems from a high-spin ferric form with effective principal $g$-values $g_z = 6.20$, $g_y = 5.9$, and $g_x = 1.98$. This form is related to protein denaturation and increases dramatically when the protein solution is aged. The last contribution to the EPR spectrum, labelled Cu, has the EPR parameters $g_\perp = 2.055$ and $g_\parallel = 2.225$, and $A_\perp = 40$ MHz and $A_\parallel = 589$ MHz for the $^{63}$Cu hyperfine coupling. These are

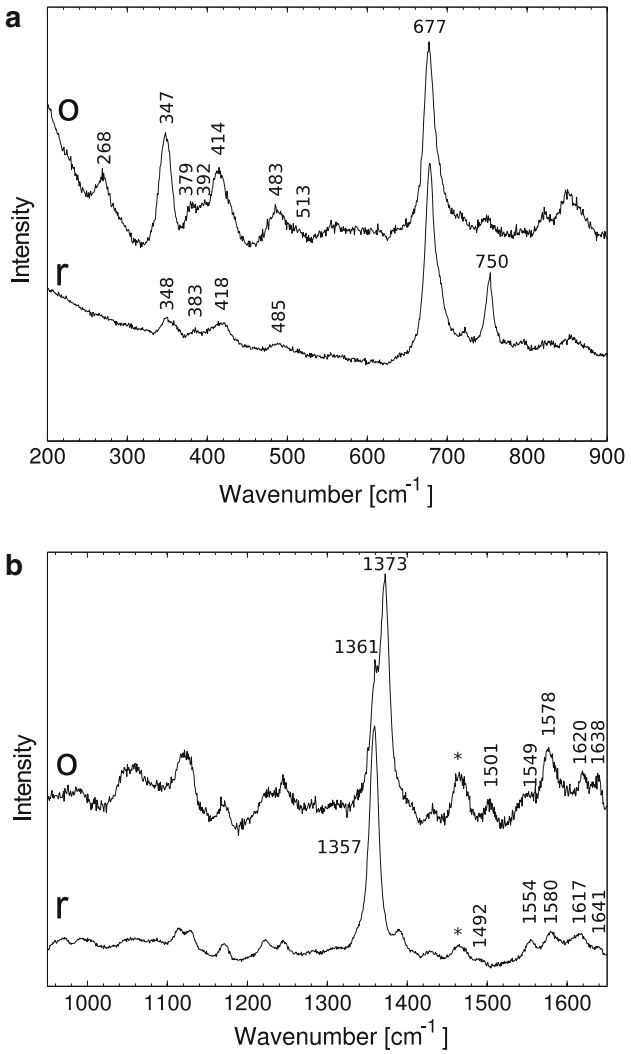


**Fig. 6a, b** Resonance Raman spectra of TSCytb in SML micelles in phosphate buffer at pH 7 and 293 K. The low-frequency (**a**) and high-frequency (**b**) region of the RR spectra of the oxidized (*o*) and the reduced (*r*) TSCytb are presented. Reduction of TSCytb was done by adding 10 µl of saturated dithionite solution to 1 ml of ~50 µM TSCytb. The *asterisk* indicates solvent modes

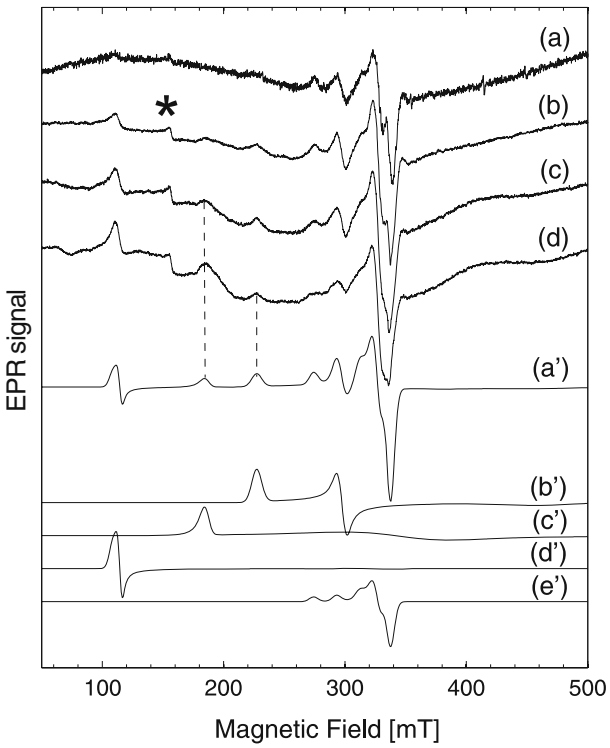


**Fig. 7** X-band CW-EPR spectra of of TSCytb in SML micelles in phosphate buffer taken at pH 7 at *a* 30 K, *b* 15 K, *c* 10 K, and *d* 5 K temperatures. The simulations of the EPR contributions of the different species: total simulated spectrum (*a*′) with components LS1 (*b*′), LS2 (*c*′), HS (*d*′), and Cu (*e*′). The simulations were performed using the EPR parameters mentioned in the text

typical of a type-II Cu(II) complex with the Cu(II) ion equatorially ligated to two to four nitrogens (Peisach and Blumberg 1974). It can be most likely ascribed to Cu(II) ions that bind to the His-tags during the purification of TSCytb.

## Discussion

Cyts-*b*561 constitutes a relatively newly identified class of proteins that is widespread in the plant and animal kingdoms (Ponting 2001; Verelst and Asard 2003; Tsubaki et al. 2005). The human genome predicts at least five Cyt-*b*561 isoforms (Tsubaki et al. 2005). Cyts-*b*561 in mammals have been implicated in such essential physiological functions as iron metabolism (McKie et al. 2001), vitamin C metabolism (Su and Asard 2006), neuropeptide synthesis (Njus and Kelley 1993; Asada et al. 2002), and tumor growth inhibition (Lerman and Minna 2000; Ji et al. 2002; Ohtani et al. 2007). Although the biological importance of Cyts-*b*561 is still poorly understood, it is obvious that it will be closely related to the biochemical activity of these proteins. Therefore, an understanding of the physicochemical properties of these di-heme proteins will significantly contribute to the detailed understanding of their physiological function.

### Absorption spectroscopy

When the split α-band in the absolute spectra of the ascorbate-reduced TSCytb was analyzed at room temperature by the SVD technique, two basic component spectra (called SVD1 and SVD2, Fig. 2d) were enough for the reconstitution of any of the ascorbate-reduced TSCytb spectra with a precision >95%. Another spectrum analysis (see also Kamensky et al. 2007) of the very same set of spectra (Fig. 2a) also revealed the presence of two spectral

components: the so-called high-affinity (or high-redox potential) and low-affinity (or low-redox potential) heme spectra.

Both the SVD1 and SVD2 spectra and the HA and the LA spectra showed a split α-band. Moreover, the separation between the two α-peaks was ~8 nm (~255 $cm^{-1}$) in the HA heme and in the SVD-1 component spectra, while it was ~6 nm (~191 $cm^{-1}$) and ~7 nm (~221 $cm^{-1}$) in the LA heme and in the SVD-2 component spectra, respectively. The contribution of the Lorentzian components to the appropriate α-band spectrum was always 50 ± 10% (Fig. 3). These results are only partly in agreement with the spectrum analysis results obtained with highly purified recombinant bovine CGCytb (Kamensky et al. 2007). For the high-potential heme spectrum of CGCytb, which is the equivalent of the HA heme spectrum, Kamensky et al. (2007) reported a split α-band with possible peak separation of ~6 nm, while the α-band in the low-potential heme spectrum was said not to be split. However, a clearly asymmetric α-band is visible in the low-potential heme spectrum (see Fig. 4b in Kamensky et al. 2007).

We have approximated each of the low-potential and high-potential heme spectra, published by Kamensky et al. (2007), with two Lorentzian absorption bands and shown that each of them can be composed from two Lorentzian absorption peaks (Table 1). The separation between the two α-peaks as well as the contribution (the weight) of the two peaks to the split α-band are different in the two component spectra. The separation of the two peaks is ~6 nm (~182 $cm^{-1}$) and ~4 nm (~125 $cm^{-1}$) in the high-potential and low-potential heme spectra, respectively. Thus the separation of the two α-peaks in the split α-band is systematically larger in spectra of TSCytb than in spectra of CGCytb.

From the principle of SVD analysis, it is clear that the SVD1 component spectrum represents the average of spectra participating in the analysis. The SVD2 component spectrum gives information on how the SVD1 component spectrum is modified at most. However, the SVD component amplitude for the SVD2 component spectrum was always at least one order of magnitude lower than that of the SVD1 component spectrum (See Fig. 2c). Further SVD component spectra thus contribute to the modification to an even much smaller extent. It is worth mentioning at this point that the spectral location of the second fitted component of the split α-band (the one at the higher wavelength) had very little variance (562.3–562.7 nm) and was independent of the kind of spectral analysis. The spectral location of the first component in the split α-band (the one at the lower wavelength), however, shifted about 2 nm from a lower wavelength value (~554.5 nm) to a higher wavelength value (~556.5 nm). Since this shift is rather smooth, we interpret this result as a sign of having one heme in a rather stable micro environment and one heme in a micro environment that is somehow influenced by the increasing concentration of ascorbate.

It has long been known that some heme proteins (among them Cyts-*b*561 as well) have an asymmetric α-band, and this band splits into two separated α-peaks in the low-temperature spectra (Hagihara et al. 1974; Kamensky and Palmer 2001). The presence of two α-peaks, however, cannot be direct evidence for the presence of two hemes in the Cyts-*b*561. Band asymmetry or spectral splitting in the $\alpha(Q_{0,0})$ absorption band can also be seen both in the low-temperature (77 K or lower) and high-temperature (270 K or higher) spectra of single-heme-containing proteins (Hagihara et al. 1974), such as cytochrome $b_5$ (Bois-Poltoratsky and Ehrenberg 1967), cytochrome $b_{562}$ (Wagner and Kassner 1975), or cytochrome *c* (Wilson 1967; Reddy et al. 1996). All the separation values of α-peaks given in Table 1 are in good agreement with values published for different one-heme-containing proteins (Reddy et al. 1996). The spectral splitting in the $\alpha(Q_{0,0})$ absorption band has been attributed to (1) distinct axial ligation arising from two porphyrin orientational isomers (La Mar et al. 1984), (2) two nearly degenerate electronic transitions and the asymmetry in the heme pocket of the protein that arises from the surrounding polypeptide chain (Reddy et al. 1996), (3) various sites produced by the alignment of electric field axes at different angles with respect to the molecular axes of the porphyrin (Leenstra 1979), or (4) the Jahn–Teller type distortions (Jahn and Teller 1937; Pearson 1975).

According to the Jahn–Teller theorem, the overall symmetry of a system will be lowered if a lower symmetry leads to a lower overall energy. All nonlinear polyatomic molecules of sufficiently high symmetry to possess orbitally degenerate electronic states will be subject to the Jahn–Teller instability. Hemes in most proteins very probably fulfill all criteria needed for experiencing the Jahn–Teller effect. However, the Jahn–Teller effect is weak when the number of *d*-electrons is five (http://en.wikipedia.org/wiki/Jahn-Teller_effect).

Since the asymmetric α-band, observable already at room temperature and at micromolar concentrations of ASC, does not split further (only experiences a blue shift) when the temperature is decreased from 297 to 77 K, the 4–8 nm separation of the two α-peak components in the reduced spectrum of Cyts-*b*561 most probably refers not to lifting the orbital degeneracy but provides experimental proof for the presence of distinct micro environments for the two hemes. The nature of the differences in the micro-environments of the two hemes in Cyts-*b*561, however, remains a subject for further studies.

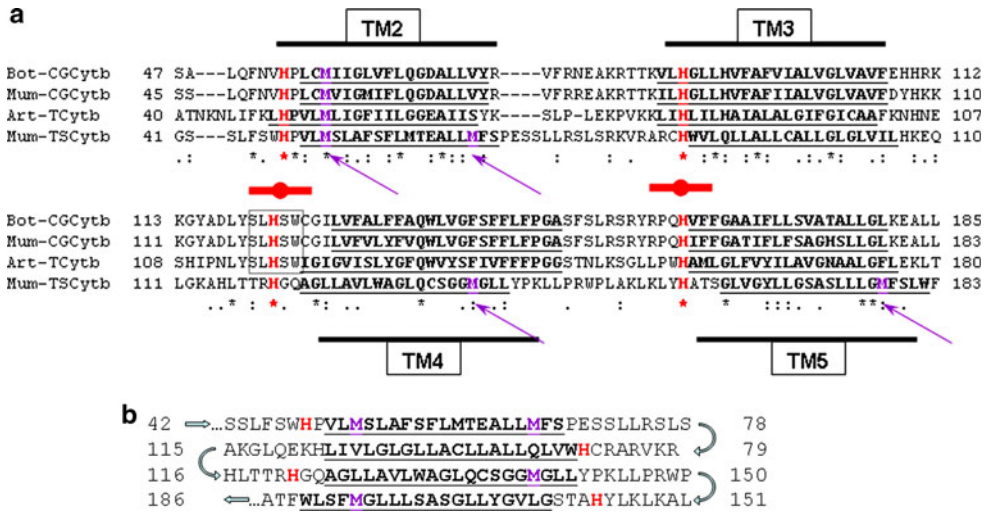


**Fig. 8** Comparison of the CB domain region of four Cyts-*b*561 for which detailed spectral analysis is available (**a**) and the CB domain of TSCytb as it might be in membranes (**b**). **a** The four highly conserved His residues (*H*), the two bis-His coordinated hemes (*red circle between dashes*),and the four consecutive *trans*-membrane helices (TM2 through TM5, *bold* and *underlined* amino acids) are shown marked in the primary sequences of bovine CGCytb (*Bot-CGCyt*), mouse CGCytb (*Mum-CGCytb*), mouse 101F6 protein (*Mum-TSCytb*), and the *Arabidopsis* tonoplast Cyt-*b*561 (*Art-TCytb*). The putative ascorbate free radical binding motif (SLHSW) is *boxed*. The *arrows* point to Met (*M*) residues mentioned. **b** The four highly conserved His residues (*H*), the four putative heme-coordinating Met residues (*M*), and the four consecutive *trans*-membrane helices (*bold* and *underlined* amino acids) are shown in the CB domain of TSCytb. *Arrows* show the consecutive reading of the amino acid sequence. Multiple alignment was obtained by CLUSTALW2 (http://www.ebi.ac.uk/Tools/clustalw2/index.html). *Trans*-membrane helices were obtained by using the HMMTOP prediction (Tusnády and Simon 1998, 2001)

## Redox potentials

For CGCytb, the redox potentials are around 50 and 150 mV, while they seem to be definitely lower for TSCytb as well as for the recombinant human 101F6 protein (Recuenco et al. 2009). The alteration might be the result of the different redox potential determination methods and/or detergents employed. However, it should be noted that the conservation of the primary structure between the two Cyts-*b*561 is rather low (Fig. 8a)—only 19% between the bovine CGCytb and the mouse TSCytb. It is well-known that even minor differences in the amino acid sequences (e.g., one point mutation) can cause differences on the order of tens of millivolts in the redox potential of hemes (Shifman et al. 2000). It seems, however, that the 100–120 mV potential difference between the redox potentials of the two hemes in Cyt-*b*561 proteins is a strong characteristic feature for these proteins.

## Resonance Raman spectroscopy

In the RR spectrum of oxidized TSCytb only a single set of Raman bands corresponding to heme skeletal and heme peripheral modes can be observed, despite the observation of two distinct low-spin ferric heme forms in the EPR spectra. This is normal, since the main difference between the two sites lies in the modes of the axial ligands (orientation of His imidazole planes), which are hardly or not observable for low-spin ferric heme proteins by RR spectroscopy. No clear evidence of the high-spin ferric species (HS) visible in the EPR spectra of TSCytb (Fig. 6) is found in the resonance Raman spectra (Fig. 5). This indicates that it constitutes a minor population in the protein sample and confirms the earlier identification of the signal as a denaturated state of the protein. Note that it is difficult to determine the relative contributions of the LS and HS ferric species in the EPR spectrum because of their large differences in electron spin and relaxation properties.

Only a single vinyl mode can be observed in the RR spectra of the ferric and ferrous TSCytb, agreeing with a lack of out-of-plane distortions of the pyrrole rings due to the rigidity of the bis-histidine coordination in both forms (Hu et al. 1996; Dewilde et al. 2006). This is corroborated by the absence of a strong band in the region of the out-of-plane $\gamma_7$ mode (290–310 $cm^{-1}$), which indicates a relaxed state where the iron lies within the porphyrin plane (Hu et al. 1996).

The fact that the photoreduction of ferric TSCytb leveled off upon increase of the laser power and no full reduction could be observed indicates that one of the hemes is resistant to photoreduction. This behavior has also been observed for neutrophil cytochrome b558 (Hurst et al. 1991) and is related to the difference in redox potential of the two hemes.

EPR spectroscopy

The EPR experiments indicate the presence of two different low-spin ferric heme species in the as-expressed TSCytb (LS1 and LS2). Although two low-spin ferric heme species were detected with EPR in CGCytb and TCytb (Tsubaki et al. 1997; Liu et al. 2005; Bérczi et al. 2005, 2007; Kamensky et al. 2007), it is remarkable that the reported $g_z$ values for the two forms in these proteins are 0.1–0.2 higher than the values obtained for LS1 and LS2 of TSCytb. The HALS species with the large $g_z$ value around 3.7 has been associated with the low potential heme in CGCytb (Liu et al. 2005; Kamensky et al. 2007). Interestingly, Kamensky and Palmer reported the observation of a HALS species with $g_z = 3.62$ in 85% reduced CGCytb (Kamensky and Palmer 2001), however, the nature and existence of this minor component has never been verified and in later work of the authors was assumed not to be a part of CGCytb (Kamensky et al. 2007).

The $g_z$ value of LS1 in TSCytb (2.96) is distinctly lower than the $g_z$ values reported for CGCytb or TCytb (3.14). Liu et al. (2005) reported that the EPR spectra of membrane fractions from *Sf9* cells expressing recombinant CGCytb recorded for the 120,000 *g* membrane fraction without prior removal of the 500 *g* membrane fraction contain a signal at $g_z = 2.9$ next to the $g_z = 3.14$ signal. The former signal disappeared when the 500 *g*-pelletable fraction was removed prior to collecting the 120,000 *g* fraction (Liu et al. 2005). In TSCytb, this cannot explain the occurrence of LS1 at $g_z = 2.96$, since TSCytb used in our measurements was purified (1) from the 4,000 $g_{max} \times 10$ min to 75,000 $g_{max} \times 60$ min microsomal membrane fraction (Bérczi and Asard 2008), which has been freed from any heavy membrane fractions, and (2) by His-tagged affinity chromatography. Moreover, the nature of the biochemical component responsible for the $g_z = 2.9$ EPR signal in the 500 *g* pellet of *Sf9* insect cells expressing recombinant CGCytb was never revealed. Furthermore, no $g_z = 3.14$ signal was observed for freshly prepared ferric TSCytb, while it was the only LS1 component observed for CGCytb samples.

Earlier work on CGCytb has shown that the local structure of the heme sites can be strongly influenced by changes in the protein structure at relatively large distances from the heme site. H54Q or H122Q mutations of CGCytb led to the disappearance of the $g_z = 3.7$ signal (identifying this signal as belonging to the low-potential heme center) and a corresponding shift of the $g_z$ value of the high-potential heme from 3.14 to 2.96 (Kamensky et al. 2007). The latter shift indicates a relaxation of the C-side heme center upon mutations involving the M-side center. Similar evidence of changes induced on the M-side heme center by mutations in the high-potential heme region has also been reported (Liu et al. 2008). Furthermore, 4.4′-dithiodipyridine (4-PDS)-treated CGCytb exhibited an EPR contribution typical of a low-spin heme *b* center with $g_z = 2.94$ that could not be reduced by ascorbate (Tsubaki et al. 2005). Similarly, an increase in pH induced a conversion of the $g_z = 3.14$ signal of CGCytb into a $g_z = 2.84$ form of a ferric species that could again not be reduced with ascorbate (Tsubaki et al. 1997). This is similar to what is found for cytochrome $b_5$, where the pH-dependent transition is related to deprotonation of one of the axial imidazole ligands or to an imidazole ligand becoming strongly hydrogen-bonded to nearby amino acid residues (Ikeda et al. 1974). It should be noted that the bis-His coordinated heme in cytochrome $b_{559}$ in its low-potential or purified form has EPR signals at $g_z = 2.93-2.94$, $g_y = 2.26-2.27$, and $g_x = 1.50-1.55$ (Babcock et al. 1985), which are almost identical to the values obtained for the LS1 of TSCytb. The current observation of the lower $g_z$ values for both low-spin ferric forms in TSCytb seems to indicate more relaxed structures for both of the hemes than those in CGCytb or TCytb. The EPR parameters of LS1 are typical for a nearly parallel orientation of the imidazole planes of the coordinating histidines, whereas the LS2 heme has nearly perpendicular orientation of these ligand planes (Quinn et al. 1987; Peisach 1998; Walker 1999).

The above analysis of the EPR spectroscopic data is entirely based on the assumption that the TSCytb protein under study indeed belongs to the Cyt-*b*561 protein class, which was based on sequence analogy, and that earlier findings on CGCytb (Liu et al. 2005; Liu et al. 2008) can be extended to the TSCytb case. TSCytb is, however, an unusually Met-rich protein and a different drawing of the CB domain of TSCytb reveals the presence of two pairs of Met residues in proper positions for heme coordination (Fig. 8b). The M52-M179 and M66-M139 Met pairs could theoretically ligate two hemes, one on each membrane side of the *trans*-membrane TSCytb. Similarly, His-Met ligations (e.g., M52-H122) of the heme could in principle be possible. Only one of these four Met residues, namely M52 (TSCytb numbering), seems to be highly conserved, and no Met residues can be found at the other three Met positions in the other Cyts-*b*561 studied in detail.

The available spectroscopic data of TSCytb cannot exclude a priori the possible presence of bis-Met or a Met-His coordination at one of the hemes in TSCytb. Although the EPR parameters of LS1 are typical for relaxed bis-histidine-coordinated heme centers, cytochrome-*c* proteins with quasi identical principal *g* values have been reported (Teixeira et al. 1993). Similarly, cytochrome-*c* proteins characterized by large $g_{max}$ values have been reported (Zopellaro et al. 2009). The absorption band at about 695 nm in the visible spectra of ferricytochromes, considered as a fingerprint for Met-His coordination (Teixeira et al. 1993), is not always observable, and its absence in the absorption spectra of TSCytb can therefore not be used as a

proof against methionine ligation. Furthermore, only a few bis-Met-coordinated hemes are known and studied by EPR spectroscopy. Bacterioferritin has bis-Met-coordinated low-spin ferri heme (Cheesman et al. 1992) with principal $g$ values of 2.86, 2.32, 1.48 (for *Pseudomonas aeruginosa*) and 2.88, 2.31, 1.46 (for *Azotobacter vinelandii*). The ligand-field parameters of the different bacterioferritins ($V/\Delta = 0.7-0.72$ and $\Delta/\lambda = 2.71-2.73$) are very similar to those of bis-thioether-coordinated iron (III) porphyrins (McKnight et al. 1991). Bis-Met ligation to heme iron was also found in mutants of cytochrome *b* (Baker et al. 1996; $g$ values 3.18, 2.25, and 0.87). Recently the streptococcal cell surface protein Shp was shown to contain a bis-Met coordinated heme with the $g_{max}$ value around 3.1 (Ran et al. 2007). The low number of examples of bis-Met coordinated heme complexes and the observed spread in their $g$ values prevents ruling out the occurrence of this ligation type based on the present spectroscopic data alone. NIR-MCD measurements (Cheesman et al. 1990; Baker et al. 1996) and/or selective point-mutation experiments in combination with EPR can give a definite answer on this ligation. These experiments are planned.

In summary, by using different spectroscopic and spectrum-analyzing techniques, we have shown the following for TSCytb: (1) its reduced spectra have a split α-band at already low ascorbate concentrations (at already high potential levels), and (2) it has two heme *b* redox centers, both with positive redox potentials, that differ by about 100 mV from each other. However, the spectroscopic parameters characterizing the state of its two heme *b* centers show observable alterations from those published earlier for TCytb and CGCytb in particular. Analyses of spectral parameters also allow us to speculate that one heme is in a rather stable micro environment while this is not so for the other heme. Finally, the recombinant mouse tumor suppressor 101F6 protein discussed in this paper seems to have redox centers with significantly higher redox potentials than the recombinant human tumor suppressor 101F6 protein, according to a very recent publication (Recuenco et al. 2009).

**Acknowledgments** The authors thank Drs. Balázs Szalontai and Csaba Bagyinka (Institute of Biophysics, BRC, Szeged, Hungary) for their help in spectrum analysis. This work was supported by grants from the University of Antwerp (to H.A.). F.D. thanks the BOF-UA-TOP fund for PhD funding.

## References

Apps DK, Pryde JG, Phillips JH (1980) Cytochrome b561 is identical with chromomembrin B, a major polypeptide of chromaffin granule membranes. Neuroscience 5:2279–2287

Apps DK, Boisclair MD, Gavine FS, Pettigrew GW (1984) Unusual redox behaviour of cytochrome *b*-561 from bovine chromaffin granule membranes. Biochim Biophys Acta 764:8–16

Asada A, Kusakawa T, Orii H, Agata K, Watanabe K, Tsubaki M (2002) Planarian cytochrome b561: conservation of a six *trans*-membrane structure and localization along the central and peripheral nervous system. J Biochem 131:175–182

Asard H, Kapila J, Verelst W, Bérczi A (2001) Higher-plant plasma membrane cytochrome *b*561: a protein in search of a function. Protoplasma 217:77–93

Babcock GT, Widger WR, Cramer WA, Oertling WA, Metz JG (1985) Axial ligands of chloroplast cytochrome *b*-559: identification and requirement for a heme-cross-linked polypeptide structure. Biochemistry 24:3638–3645

Baker PD, Nerou EP, Cheesman MR, Thomson AJ, de Oliveira P, Hill HAO (1996) Bis-Methionine ligation to heme iron in mutants of cytochrome *b*. 1. Spectroscopic and electrochemical characterization of the electronic properties. Biochemistry 35:13618–13626

Bashtovyy D, Bérczi A, Asard H, Páli T (2003) Structure prediction for di-heme cytochrome *b*561 protein family. Protoplasma 221:31–40

Bérczi A, Asard H (2008) Expression and purification of the recombinant mouse tumor suppressor cytochrome *b*561 protein. Acta Biol Szeged 52:257–265

Bérczi A, Su D, Lakshminarasimhan M, Vargas A, Asard H (2005) Heterologous expression and site-directed mutagenesis of an ascorbate-reducible cytochrome *b*561. Arch Biochem Biophys 443:82–92

Bérczi A, Su D, Asard H (2007) An *Arabidopsis* cytochrome *b*561 with *trans*-membrane ferrireductase capability. FEBS Lett 581:1505–1508

Blumberg WE, Peisach J (1971) A unified theory for low-spin forms of all ferric heme proteins as studied by EPR. In: Chance B, Yonetani T, Mildvan AS (eds) Probes of structure and function of macromolecules and membranes. Probes of enzymes and hemoproteins, vol 2. Academic Press, New York, pp 215–229

Bois-Poltoratsky R, Ehrenberg A (1967) Magnetic and spectrophotometric investigations of cytochrome $b_5$. Eur J Biochem 2: 361–365

Branca RMM, Bodó G, Várkonyi Z, Debreczeny M, Ősz J, Bagyinka C(2007) Oxygen and temperature-dependent structural and redox changes in a novel cytochrome $c_4$ from the purple sulfur photosynthetic bacterium *Thiocapsa roseopersicina*. Arch Biochem Biophys 467:174–184

Cerda-Colon JF, Silfa E, Lopez-Garriga J (1998) CO-dependent activity controlling mechanism of heme-containing CO-sensor protein, NPAS2. J Am Chem Soc 120:9312–9317

Cheesman MR, Thomson AJ, Greenwood C, Moore GR, Kadir F (1990) Bis-methionine axial ligation of haem in bacterioferritin from *Pseudomonas aeruginosa*. Nature 346:771–773

Cheesman MR, Kadir FHA, Al-Basseet J, Al-Massad F, Farrar J, Greenwood C, Thomson AJ, Moore GF (1992) E.P.R. and magnetic circular dichroism spectroscopic characterization of bacterioferritin from *Pseudomonas aeruginosa* and *Azotobacter vinelandii*. Biochem J 286:361–367

Dewilde S, Ebner B, Vinck E, Gilany K, Hankeln T, Burmester T, Kreiling J, Reinisch C, Vanfleteren JR, Kiger L, Marden MC, Hundahl C, Fago A, Van Doorslaer S, Moens L (2006) The nerve hemoglobin of the bivalve mollusc *Spisula solidissima*: molecular cloning, ligand binding studies, and phylogenetic analysis. J Biol Chem 281:5364–5372

Flatmark T, Grønberg M (1981) Cytochrome *b*-561 of the bovine adrenal chromaffin granules. Molecular weight and hydrodynamic properties in micellar solutions of Triton X-100. Biochem Biophys Res Commun 99:292–301

Flatmark T, Terland O (1971) Cytochrome $b_{561}$ of the bovine adrenal chromaffin granules. A high potential b-type cytochrome. Biochim Biophys Acta 253:487–491

Fleming PJ, Kent UM (1991) Cytochrome b561, ascorbic acid, and transmembrane electron transfer. Am J Clin Nutr 54:1173S–1178S

Griesen D, Su D, Bérczi A, Asard H (2004) Localization of an ascorbate-reducible cytochrome *b*561 in the plant tonoplast. Plant Physiol 134:726–734

Hagihara B, Oshino R, Iizuka T (1974) Studies on low temperature spectra of respiratory pigments. II. Spectra of cytochromes in respiratory systems between liquid helium and room temperatures. J Biochem 75:45–51

Henry ER, Hofrichter J (1992) Singular value decomposition: application to analysis of experimental data. Meth Enzymol 210:129–193

Hu S, Morris IK, Singh JP, Smith KM, Spiro TG (1993) Complete assignment of cytochrome *c* resonance Raman spectra via enzymatic reconstitution with isotopically labeled hemes. J Am Chem Soc 115:12446–12458

Hu S, Smith KM, Spiro TG (1996) Assignment of protoheme resonance Raman spectrum by heme labeling in myoglobin. J Am Chem Soc 118:12638–12646

Hurst B, Loehr TM, Curnutte JT, Rosen H (1991) Resonance Raman and electron paramagnetic resonance structural investigations of neutrophil cytochrome $b_{558}$. J Biol Chem 266:1627–1634

Ikeda M, Iizuka T, Takao H, Hagihara B (1974) Studies on heme environment of oxidized cytochrome $b_5$. Biochim Biophys Acta 226:15–24

Jahn HA, Teller E (1937) Stability of polyatomic molecules in degenerate electronic states. I. Orbital degeneracy. Proc R Soc Lond Ser A 161:220–235

Ji L, Nizhizaki M, Gao B, Burbee D, Kondo M, Kamibayashi C, Xu K, Yen N (2002) Expression of several genes in the human chromosome 3p21.3 homozygous deletion region by an adenovirus vector results in tumor suppressor activities in vitro and in vivo. Cancer Res 62:2715–2720

Kamensky YA, Palmer G (2001) Chromaffin granule membranes contain at least three heme centers: direct evidence from EPR and absorption spectroscopy. FEBS Lett 491:119–122

Kamensky Y, Liu W, Tsai A-L, Kulmacz RJ, Plamer G (2007) Axial ligation and stoichiometry of heme centers in adrenal cytochrome b561. Biochemistry 46:8647–8658

Kelley PM, Njus D (1986) Cytochrome b561 spectral changes associated with electron transfer in chromaffin-vesicle ghosts. J Biol Chem 261:6429–6432

Kent UM, Fleming PJ (1987) Purified cytochrome $b_{561}$ catalyzes transmembrane electron transfer for dopamine $\beta$-hydroxylase and peptidyl glycine $\alpha$-amidating monooxygenase activities in reconstituted systems. J Biol Chem 262:8174–8178

La Mar GN, Toi H, Krishnamoorthi R (1984) Proton NMR investigation of the rate and mechanism of heme rotation in sperm whale myoglobin: evidence for intramolecular reorientation about a heme two-fold axis. J Am Chem Soc 106:6395–6401

Leenstra WR (1979) The triplet state of porphyrins. Ph.D. Thesis, University of Washington, Seattle, WA, USA

Lerman MI, Minna JD (2000) The 630-kb lung cancer homozygous deletion region on human chromosome 3p21.3: identification and evaluation of the resident candidate tumor suppressor genes. Cancer Res 60:6116–6133

Liu W, Kamensky Y, Kakkar R, Foley E, Kulmacz RJ, Palmer G (2005) Purification and characterization of bovine adrenal cytochrome b561 expressed in insect and yeast cell systems. Protein Expr Purif 40:429–439

Liu W, Rogge CE, Kamensky Y, Tsai A-L, Kulmacz RJ (2007) Development of a bacterial system for high yield expression of fully functional adrenal cytochrome $b_{561}$. Protein Expr Purif 56:145–152

Liu W, Rogge CE, da Silva GFZ, Shinkarev VP, Tsai A-L, Kamensky Y, Palmer G, Kulmacz RJ (2008) His92 and His110 selectively affect different heme centers of adrenal cytochrome b561. Biochim Biophys Acta 1777:1218–1228

Lou BS, Snyder JK, Marshall P, Wang JS, Wu G, Kulmacz RJ, Tsai AL, Wang J (2000) Resonance Raman studies indicate a unique heme active site in prostaglandin H synthase. Biochemistry 39:12424–12434

Markwell MAK, Haas SB, Bieber LL, Tolbert NE (1978) A modification of the Lowry procedure to simplify protein determination in membrane and lipoprotein samples. Anal Biochem 87:206–210

McKie AT, Barrow D, Latunde-Dada GO, Rolfs A, Sager G, Mudaly E, Mudaly M, Richardson C, Barlow D, Bomford A, Peters RJ, Raja KB, Shirali S, Hediger MA, Farzaneh F, Simpson RJ (2001) As iron-regulated ferric reductase associated with the absorption of dietary iron. Science 291:1755–1759

McKnight J, Cheesman MR, Reed CA, Orosz R, Thomson AJ (1991) Comparative study of the optical and magnetic circular dichroism spectra of bis-thioether and -imidazole complexes of iron(III) tetraphenyl and octaethyl-porphyrin. Models of haem coordination in bacterioferritins. J Chem Soc Dalton Trans 1991(8):1887–1894

Mizutani A, Sanuki R, Kakimoto K, Kojo S, Taketani S (2007) Involvement of 101F6, a homologue of cytochrome $b_{561}$, in the reduction of ferric ions. J Biochem 142:699–705

Njus D, Kelley PM (1993) The secretory-vesicle ascorbate-regenerating system: a chain of concerted H+/e(−)-transfer reactions. Biochim Biophys Acta 1144:235–248

Ohtani O, Iwamaru A, Deng W, Ueda K, Wu G, Jayachandran G, Kondo S, Atkinson EN, Minna JD, Roth JA, Ji L (2007) Tumor suppressor 101F6 and ASC synergistically and selectively inhibit non–small cell lung cancer growth by caspase-independent apoptosis and autophagy. Cancer Res 67:6293–6303

Pearson RG (1975) Concerning Jahn-Teller effects. Proc Natl Acad Sci USA 72:2104–2106

Peisach J (1998) EPR of metalloproteins: truth tables revisited. In: Eaton GR, Eaton SS, Salikov K (eds) Foundations of modern EPR, 1st edn. World Scientific Publishing, Singapore, pp 346–360

Peisach J, Blumberg WE (1974) Structural implications derived from the analysis of electron paramagnetic resonance spectra of natural and artificial copper proteins. Arch Biochem Biophys 165:691–708

Ponting CP (2001) Domain homologues of dopamine $\beta$-hydroxylase and ferric reductase: roles for iron metabolism in neurodegenerative disorders. Human Mol Gen 10:1853–1858

Quinn R, Valentine JS, Byrn MP, Strouse CE (1987) Electronic structure of low-spin ferric porphyrins: a single-crystal EPR and structural investigation of the influence of axial ligand orientation and the effects of pseudo-Jahn-Teller distortion. J Am Chem Soc 109:3301–3308

Ran Y, Zhu H, Liu M, Fabian M, Olson JS, Aranda R IV, Phillips GN, Dooley DM, Lei B (2007) Bis methionine ligation to heme iron in the streptococcal cell surface protein Shp facilitates rapid hemin transfer to HtsA of the HtsABC transporter. J Biol Chem 282:31380–31388

Recuenco MC, Fujito M, Rahman M, Sakamoto Y, Takeuchi F, Tsubaki M (2009) Functional expression and characterization of human 101F6 protein, a homologue of cytochrome b561 and a candidate tumor suppressor gene product. Biofactors 34:219–230

Reddy KS, Angiolillo PJ, Wright WW, Laberge M, Vanderkooi JM (1996) Spectral splitting in the $\alpha$(Q0,0) absorption band of ferrous cytochrome c and other heme proteins. Biochemistry 35:12820–12830

Shifman JM, Gibney BR, Sharp RE, Dutton PL (2000) Heme redox potential control in *de novo* designed four-α-helix bundle proteins. Biochemistry 39:14813–14821

Shrager RI (1986) Chemical transitions measured by spectra and resolved using singular value decomposition. Chem Intell Lab Syst 1:59–70

Stoll S, Schweiger A (2006) EasySpin, a comprehensive software package for spectral simulation and analysis in EPR. J Magn Reson 178:42–55

Su D, Asard H (2006) Three mammalian cytochrome $b_{561}$ are ascorbate dependent ferrireductases. FEBS J 273:3722–3734

Takeuchi F, Kobayashi K, Tagawa S, Tsubaki M (2001) Ascorbate inhibits the carbethoxylation of two histidyl and one tyrosyl residues indispensable for the transmembrane electron transfer reaction of cytochrome *b*561. Biochemistry 40:4067–4076

Takeuchi F, Hori H, Obayashi E, Shiro Y, Tsubaki M (2004) Properties of two distinct centers of cytochrome *b*561 from bovine chromaffin vesicles studied by EPR, resonance Raman, and ascorbate reduction assay. J Biochem 135:53–64

Taylor CPS (1977) The EPR of low spin heme complexes. Relation of the $t_{2g}$ hole model to the directional properties of the g-tensor, and a new method for calculating the ligand field parameters. Biochim Biophys Acta 491:137–149

Teixeira M, Campos AP, Aguiar AP, Costa HS, Santos H, Turner DL, Xavier AV (1993) Pitfalls in assigning heme axial coordination by EPR. C-type cytochromes with atypical Met-His ligation. FEBS Lett 317:233–236

Terekhov SN, Kruglik SG (1995) Photoreduction of ferric-tetraphenylporphyrin in oxygen-containing solvents revealed by resonance Raman and absorption spectroscopy. Chem Phys Lett 245:268–272

Tsubaki M, Nakayama M, Okuyam E, Ichikawa Y, Hori H (1997) Existence of two heme B centers in cytochrome *b*561 from bovine adrenal chromaffin vesicles as revealed by a new purification procedure and EPR spectroscopy. J Biol Chem 272:23206–23210

Tsubaki M, Takeuchi F, Nakanashi N (2005) Cytochrome *b*561 protein family: expanding roles and versatile transmembrane electron transfer abilities as predicted by a new classification system and protein sequence motif analyses. Biochim Biophys Acta 1753:174–190

Tusnády GE, Simon I (1998) Principles governing amino acid composition of integral membrane proteins: application to topology prediction. J Mol Biol 283:489–506

Tusnády GE, Simon I (2001) The HMMTOP transmembrane topology prediction server. Bioinformatics 17:849–850

Uchida T, Sato E, Sato A, Sagami I, Shimizu T, Kitagawa T (2005) CO-dependent activity-controlling mechanism of heme-containing CO-sensor protein, neuronal PAS domain protein 2. J Biol Chem 280:21358–21368

Verelst W, Asard H (2003) A phylogenetic study of cytochrome *b*561 proteins. Genome Biol 4:R38

Wagner GC, Kassner RJ (1975) Spectroscopic properties of low-spin ferrous heme complexes and heme proteins at 77°K. Biochem Biophys Res Commun 63:385–391

Wakefield LM, Cass AEG, Radda GK (1984) Isolation of a membrane protein by chromatofocusing: Cytochrome *b*-561 of the adrenal chromaffin granule. J Biochem Biophys Methods 9:331–341

Walker FA (1999) Magnetic spectroscopic (EPR, ESEEM, Mössbauer, MCD and NMR) studies of low-spin ferriheme centers and their corresponding heme proteins. Coord Chem Rev 185–186:471–534

Wilson DF (1967) Effect of temperature on the spectral properties of some ferrocytochromes. Arch Biochem Biophys 121:757–768

Zhang D, Su D, Bérczi A, Vargas A, Asard H (2006) An ascorbate-reducible cytochrome *b*561 is localized in macrophage lysosomes. Biochim Biophys Acta 1760:1903–1913

Zopellaro G, Bren KL, Ensign AA, Herbitz E, Kaur R, Hersleth HP, Ryde U, Hederstedt L, Andersson KK (2009) Studies of ferric heme proteins with highly anisotropic/highly axial low spin (S = 1/2) electron paramagnetic resonance signals with bis-histidine and histidine-methionine axial iron coordination. Biopolymers. doi: 10.1002/bip.21267